

The Ba 4d-f giant dipole resonance as a probe of the structure of endohedral Ba@C_n metallofullerenes

Jarek Luberek and Göran Wendin

Department of Applied Physics, Chalmers University of Technology

S-412 96 Göteborg, Sweden

(June 28, 2021)

Abstract

We calculate the x-ray absorption near edge structure (XANES) modulating the Ba 4d-photoabsorption cross section - the giant dipole resonance - centered around 110 eV photon energy for several models of spherical and *non-spherical* Ba@C_n metallofullerene cage systems. In the cases considered, the XANES interference patterns provide clear structural "fingerprints", distinguishing between center versus off-center Ba position and spherical versus deformed C_n shell.

Cage molecules are well known for spectacular interference effects, causing very pronounced structure in photoabsorption cross sections. Nearly ideal cages should be provided by fullerene molecules C_n , $n = 60, 70, \dots$, in gas phase or in solid form. Among various forms of doped fullerenes, there is the possibility to put metal atoms inside C_n , endohedral metallofullerenes - $M@C_n$ [1]. Recently there has been a wealth of reports on the preparation and characterization of endohedral metallofullerenes $M@C_n$ [2,3,4] as well as calculations of structure, affinity and ionization energies [5,6,7].

The presence of a heavy metal atom inside a cage of ligands provides a very interesting many-electron system: the collective dynamics of the coupled many-electrons systems may give rise to giant dipole resonances, and single-particle multiple scattering will lead to standing wave patterns and resonances inside the cage [8,9]. As a result, the broad giant dipole resonance will be modulated by x-ray absorption near edge structure (XANES) as illustrated by the Ba 4d-photoionization cross section in solid BaF_2 and $YBaCuO$ (see e.g. ref. [10]).

In this Letter we present results from an investigation of the collective and single-electron response in photoemission from the 4d core level of a Ba atom placed inside a model fullerene cage in cases of spherical and *non-spherical* symmetry. We focus attention on two situations: (i) a Ba atom displaced from the center of a spherical C_{60} model cage, $Ba@C_{60}(C_{\infty v})$, and (ii) a Ba atom at the center of a non-spherical cage consisting of a short tube with hemispherical endcaps, to be referred to as $Ba@C_{90}(D_{\infty h})$. We find that the multiple scattering structure of the photoabsorption cross section is a sensitive probe of the position of the emitter atom and the shape of the cage. We propose that the oscillations of the 4d-f giant dipole resonance can provide a characteristic "fingerprint" of the system - distinguishing almost by inspection between center vs off-center position of the Ba emitter atom as well as spherical vs non-spherical shape of the cage.

The $Ba@C_n$ structure is defined by a point charge $Z_{Ba} = 56$ for the Ba nucleus and a surface effective nuclear charge Z_{shell} for the C_n shell [8]. In this way the nuclear point charges of the real C_n structure is averaged to a homogeneous surface charge distribution

corresponding to the number of carbon valence electrons (4 per C-atom). This is in fact an effective 2-dimensional jellium model. We then fill in the appropriate number $N = Z_{\text{Ba}} + Z_{\text{shell}}$ of electrons for a neutral $\text{Ba}@C_n$ cluster and calculate the electronic structure selfconsistently within the local-density approximation (LDA) (the structure and dynamics of spherical $\text{La}@C_{60}$ was studied in the same way by Wästberg and Wendin [9]).

To find the electronic structure of a *non-spherical* cluster we expand the initial bound state wave functions $\psi(\mathbf{r}) = (1/r) \sum_L u_L(r) Y_L(\Omega)$ and the final state Green functions $G(\mathbf{r}, \mathbf{r}', E) = \sum_{L, L'} Y_L(\Omega) G_{L, L'}(r, r') Y_{L'}^*(\Omega')$, $L = (l, m)$, in spherical harmonics around the center of the heavy central atom [11,12]. In such a one-center expansion, the molecular problem reduces to an atomic problem, but with coupled angular-momentum channels. The advantage is that the Coulomb interaction can be expressed in terms of spherical harmonics, which allows straightforward calculation of the dielectric response function. Hence electron-electron correlation and many-particle dynamics in the cluster can be studied using well established many-body techniques for atomic systems.

The resulting coupled radial Schrödinger equations were solved by procedures described in Ref. [12]. From the spherical expansion of initial state wave functions and final state Green functions [13] we then construct the dielectric susceptibility $\chi_0(\mathbf{r}, \mathbf{r}'; \omega)$ and calculate the induced charge $\delta n(\mathbf{r}; \omega)$ in a self-consistent manner within the TDLDA (time dependent local density approximation) [14]. We finally obtain the photoabsorption cross section $\sigma(\omega) \sim \omega \text{Im} \int z \delta n(\mathbf{r}; \omega) dr$ where $z = r \cos \theta$ is the electric dipole operator [15] with the electric field along the z-axis. In this work the polarization vector is always chosen along the rotational symmetry axis [16].

Figure 1 shows the electronically selfconsistent (SCF) (fixed geometry) ground state charge densities for the three different model systems we consider. Figure 1(a) shows the electronic density of spherically symmetric $\text{Ba}@C_{60}$, Fig.1(b) shows the case of $\text{Ba}@C_{60}(\text{C}_{\infty v})$ with Ba displaced from the center of a spherically symmetric C_{60} cage, and Fig.1(c) shows the symmetric case of $\text{Ba}@C_{90}(\text{D}_{\infty h})$, where the cage is a short cylinder with hemispherical C_{60} endcaps. The radius of the Ba 5s/5p charge density is about 2.5 a.u., corresponding

to the radius of the well isolated central charge density of the Ba^{2+} ion core (black spot) in Figs.(1a)-(1c). In contrast, the Ba 6s-radius is about 6 a.u., causing large 6s-amplitude between Ba the C_n shell. The calculated low charge density in this bond region suggests that the two Ba 6s valence electrons have been transferred to the C_n shell, leaving a doubly ionized central Ba^{2+} ion, ($\text{Xe } 4d^{10}5s^25p^6$ configuration), with some weak effects of bond formation in the displaced case in Fig.1(b). In the case of $\text{Ba}@\text{C}_{90}$ in Fig.1(c), the strongly ionic character is particularly evident.

The geometries in Fig.1 do not necessarily represent equilibrium positions. In fact, we have calculated the variation of the total energy for $\text{Ba}@\text{C}_{60}$ as a function of displacement of the Ba atom. Technically, the shell is displaced, and we study the variation of $E_{\text{tot}}(\text{Ba}@\text{C}_{60}) - E_{\text{tot}}(\text{C}_{60})$ to minimize systematic errors from the finite l -expansion. As a result we find that there is a small lowering of E_{tot} when the Ba atom is displaced from the center of C_{60} . Since we have not allowed any freedom in the shape and structure of the C_{60} shell, we cannot draw any firm conclusions. However, our results suggest that here is a tendency for the Ba atom to have an off-center equilibrium position, in agreement with calculations for $\text{La}@\text{C}_{82}$ [6], $\text{Ce}@\text{C}_{82}$ [7] and $\text{Ca}@\text{C}_{60}$ [3]. It might even be appropriate to regard the metal atom as "adsorbed" on the inside of the fullerene cage.

Figure 2 shows a central result of this Letter, namely the photoabsorption (total photoionization) cross sections $\sigma(\omega)$ of the $\text{Ba}@\text{C}_n$ clusters described in Fig. 1. The electric field vector is along the rotational symmetry axis in displaced $\text{Ba}@\text{C}_{60}(\text{C}_{\infty v})$ and along the cylinder (long) axis in elongated $\text{Ba}@\text{C}_{90}(\text{D}_{\infty h})$.

From our previous work [8,11] we know that the environment does not modify the overall strength and shape of the Ba $4d - \epsilon f$ ($4d - 4f$) giant dipole resonance: the effect is to induce a structure which oscillates around the atomic "background". The three curves in Fig.2 nevertheless present three easily distinguishable patterns - or "fingerprints" - which may serve as a guide to the structure of the local environment:

- (i) The spherical $\text{Ba}@\text{C}_{60}$ case (Fig.1(a)) is simple: the pronounced XANES oscilla-

tions present a clear signature of the unique distance of a single coordination shell. These oscillations must be associated with additional nodes of the continuum ϵf -wave function moving through the C_{60} shell into a radial standing wave in the inner region outside the Ba core. This f-wave function must be of a molecular, multiple scattering, kind connected with large-amplitude shape resonances, and cannot be described in terms of single scattering.

(ii) The non-spherical, displaced, $Ba@C_{60}(C_{\infty v})$ case (Fig.1(b)) lacks pronounced oscillations and, at first sight, even characteristic structure seems to be absent. However, the shape of the 4d cross section is quite different from that of a free Ba atom superimposed on a C_{60} background [8] (which corresponds to averaging out the oscillations in $Ba@C_{60}$ in case (i) above). With a displaced Ba atom there are now obviously two characteristic distances along the electric field vector: a short "bond" distance of about 5 a.u. and a long distance of about 8.4 a.u. A closer inspection of Fig.2 suggests that the XANES peaks in case (i) have been shifted towards higher energies, perhaps due to the a dominating influence of the shortest Ba – C_{60} "bond" distance.

(iii) The non-spherical, but inversion symmetric, $Ba@C_{90}(D_{\infty h})$ case (Fig.1(c)) lacks pronounced XANES oscillations but nevertheless shows considerable characteristic structure. There is no single unique coordination distance, but - as will be demonstrated below - one can observe structure due to standing waves along the cylinder (long) axis.

To illuminate the electric-field polarization dependence of the XANES we compare the cylindrical, cigar-shaped $Ba@C_{90}(D_{\infty h})$ with the corresponding inscribed (short axis) and circumscribed (long axis) spherical systems. The inscribed system we have already discussed - $Ba@C_{60}$. The circumscribed model system is provided by a spherically symmetric $Ba@C_{130}$ cluster (522 electrons in the isolated jellium shell). $Ba@C_{130}$ is designed to have a unique coordination length equal to the long axis of $Ba@C_{90}$ - the question is whether this similarity will show up in the XANES.

In Fig. 3, the similarity between $Ba@C_{130}$ and $Ba@C_{90}$ is striking: the peak portion of the $Ba@C_{90}$ cross section looks very similar to that of $Ba@C_{130}$ with the oscillations averaged out. This suggests that the flat-topped giant 4d-dipole resonance of $Ba@C_{90}$ does

reflect the narrow distribution of coordination distances defined by the long axis. Moreover, since Ba@C₆₀ corresponds to the short axis and Ba@C₁₃₀ to the long axis of Ba@C₉₀, Fig.3 suggests that there will be constructive interference at the Ba nucleus (4d-shell) around 110 and 140 eV photon energy and destructive interference around 120 -130 eV, as indeed seems to be the case in the Ba@C₉₀ cross section.

Figure 3 also allows comparison of the XANES of the spherical Ba@C₆₀ and Ba@C₁₃₀ systems. The immediate impression of the oscillating structures is that they arise from standing waves inside the shells, and that the wavelengths must correspond to the radii of the shells. Plotted on a final state momentum scale $k = \sqrt{\epsilon} = \sqrt{\omega + E_{4d}}$, in both cases the peaks appear as roughly equally spaced above $\omega = 110$ eV. In the simplest of models we may try to associate the peaks with high-lying resonances in a radial quantum well, $kR = n\pi + \text{const}$, $R = \pi/\delta k$. In this way $R(\text{Ba@C}_{60}) \approx 7\text{-}9$ a.u. and $R(\text{Ba@C}_{130}) \approx 9\text{-}11$ a.u., in reasonable agreement with the given radii of the shells (6.7 and 10 a.u, resp), but with considerable variations from peak to peak. Therefore, even if the XANES oscillations look nice and regular, they cannot be used for precise structure determination in the spirit of high-energy EXAFS (extended X-ray absorption fine structure).

We are not aware of any experimental results for endohedral metallofullerene systems that can be compared with the present theoretical photoabsorption cross sections. However, it is a fact that the 4d-giant dipole resonance in the high- T_c superconductor YBaCuO (Ba in a cage of 6-fold coordinated O; Ba-O distance about 5.1 a.u.) looks very similar to the case of spherically symmetric Ba@C₆₀ [8] shown in Fig.1. To be able to observe such strong oscillations in metallofullerens, according to the present investigation the metal atom must sit at the center of a spherical cage (unique coordination distance). Since this is not likely to occur for Ba@C₆₀, because the cage is too large and the Ba atom will sit at an off-center position, it might be necessary to laser evaporate the C_n fullerene cage and shrink it down to, say, Ba@C₄₄ (in analogy with La@C₄₄ [4]). In this case the cage radius ($R \approx 5.7$ a.u.) will correspond more closely to a natural chemical bonding distance - possibly this is the case that will compare most directly with the XANES-modulated 4d-giant dipole resonance

in YBaCuO.

Finally, in Fig.4 we present partial photoionization cross sections of displaced $\text{Ba@C}_{60}(\text{C}_{\infty v})$. As expected, the 4d-f giant dipole resonance shows up in all of the 4d, 5s, 5p and valence level photoemission cross sections with their usual characteristic resonance profiles: $n = 4$ subshells roughly follow the 4d-f resonance, while $n \geq 5$ subshells (which are basically *outside* the 4d-f dipole) show their resonance enhancement on the rising edge of the 4d-f giant dipole resonance. The weak hump at around 125 eV, discussed above, can be seen in all of the emission channels. The valence emission shows resonance enhancement around 100-110 eV at the same position as the emission from the 5s and 5p orbitals, and then goes over into "background" emission from the C_{60} shell. This indicates significant hybridization of the C_{60} shell with Ba 5d orbitals, in line with the recent photoemission results for solid Ba_6C_{60} by Knupfer et al. [17,16] and with calculations for Ba_6C_{60} [19,20].

In fact, our complete results show that the two highest occupied molecular orbitals (HOMO) have 4f-character on Ba while the next lower orbitals have 5d- and 6s/6p-character. This follows in two ways: (i) direct inspection (or partial-wave analysis) shows that the valence orbital character on Ba is mainly that of (distorted) Ba 4f, 5d and 6s/6p; (ii) the partial cross sections show resonance enhancement of the kind demonstrated in Fig.4 - the one for the 4f-hybridized orbitals looks similar to the 4d-cross section, while the ones for the 5d- and 6s/6p-hybridized orbitals look similar to the 5s/5p cross sections. In this way we have a very useful connection between the character of the initial orbital of the photoemitted electron and the frequency dependence of the photoelectron intensity.

In conclusion, we have applied a TDLDA one-center expansion to a model of a non-spherical metallofullerene cage system - Ba@C_n - in order to study the combined effects of dynamic screening, multiple scattering and non-spherical local environment on the collective Ba 4d-giant dipole resonance centered around 110 eV photon energy. For the geometries selected in this work, the XANES show distinctly different patterns, distinguishing almost by inspection between center versus off-center position of the Ba emitter atom as well as spherical versus non-spherical shape of the cage. Our results directly concern photoabsorp-

tion and photemission from oriented samples - e.g. solids or adsorbates - with polarization vectors along the high-symmetry rotation axis. However, our analysis suggests that significant parts of the corresponding XANES will be recognizable also in gas phase spectra. Whether these XANES signatures are robust enough to serve as unambiguous "fingerprints" in general situations can only be decided by comparison with future experimental results. It would be useful to have photoionization cross sections for $\text{Xe}@C_n$ [21] and surrounding elements, e.g. $\text{Sn}@C_n$ - $\text{Ce}@C_n$, representing different cases of bonding and charge transfer, shapes of 4d-giant dipole resonances, and many-electron effects.

We would like to thank Zachary H. Levine and Bo Wästberg for invaluable support. We are grateful to R.N. Compton, J. Pendry and Z.C. Ying for illuminating communications. This work has been supported by the Swedish Natural Science Research Council and the National Supercomputer Centre in Sweden.

REFERENCES

- [1] H.W. Kroto et al., Nature **318**, 162 (1985); J.R. Heath et al., J. Am. Chem. Soc **107**, 7779 (1985).
- [2] D.S. Bethune et al., Nature **366**, 123 (1993) and references therein.
- [3] L.S. Wang et al., Chem. Phys. Lett. **207**, 354 (1993).
- [4] R. Huang et al., Chem. Phys. Lett. **228**, 311 (1994).
- [5] A. Rosén and B. Wästberg, J. Am. Chem. Soc. **110**, 8701 (1988); J. Chem. Phys. **90**, 2525 (1989); B. Wästberg and A. Rosén, Physica Scripta **44**, 276 (1991).
- [6] K. Laasonen, W. Andreoni, and M. Parrinello, Science **258**, 1918 (1992).
- [7] S. Nagase and K. Kobayashi, Chem. Phys. Lett. **228**, 106 (1994).
- [8] G. Wendin and B. Wästberg, Phys. Rev. B **48**, 14764 (1993), and references therein.
- [9] B. Wästberg and G. Wendin, Nucl. Inst. and Meth. B **87**, 124 (1994).
- [10] M. Onellion et al., Phys. Rev. B **36**, 819 (1987).
- [11] Z. Crljen, J. Luberek, G. Wendin and Z.H. Levine, Phys. Rev. A **50**, 3529 (1994), and references therein.
- [12] Z.H. Levine and P. Soven, Phys. Rev. Lett. **50**, 2074 (1983); Z.H. Levine and P. Soven, Phys. Rev. A **29**, 625 (1984); **35**, 3964 (1987) (E); Z.H. Levine, Phys. Rev. A **30**, 1120 (1984).
- [13] The L -expansions for the wave and Green functions were well converged for $l_{\max} = 14$ in displaced $\text{Ba}@\text{C}_{60}(\text{C}_{\infty v})$ and for $l_{\max} = 17$ in elongated $\text{Ba}@\text{C}_{90}(\text{D}_{\infty h})$ (there is no singularity in the potential of the C_n shell).
- [14] A. Zangwill and P. Soven, Phys. Rev. A **21**, 1561 (1980).
- [15] Corrections to the dipole approximation will be of order $(R/\lambda)^2$. In the worst case, the

C_n shell, the ratio of the diameter ($R \sim 1$ nm) to the wavelength ($\lambda \sim 10$ nm) is ~ 0.1 . Therefore, the dipole approximation is an excellent approximation for the systems considered.

- [16] Although straightforward, the case of x/y-polarization (low symmetry direction) is computationally much more demanding and beyond the scope of the present work.
- [17] M. Knupfer, F. Stepniak, and J.H. Weaver, Phys. Rev. B **49**, 7620 (1994).
- [18] In Ba_6C_{60} the Ba atoms are located inside interstitial pockets formed in the bcc C_{60} lattice. Roughly speaking, Ba atoms are "adsorbed" on the *outside* of the C_{60} shells in bridging positions.
- [19] S.C. Erwin and M.R. Pederson, Phys. Rev. B **47**, 14657 (1993).
- [20] S. Saito and A. Oshiyama, Phys. Rev. Lett. **71**, 121 (1993).
- [21] M. Saunders et al., J. Am. Chem. Soc. **116**, 2193 (1994).

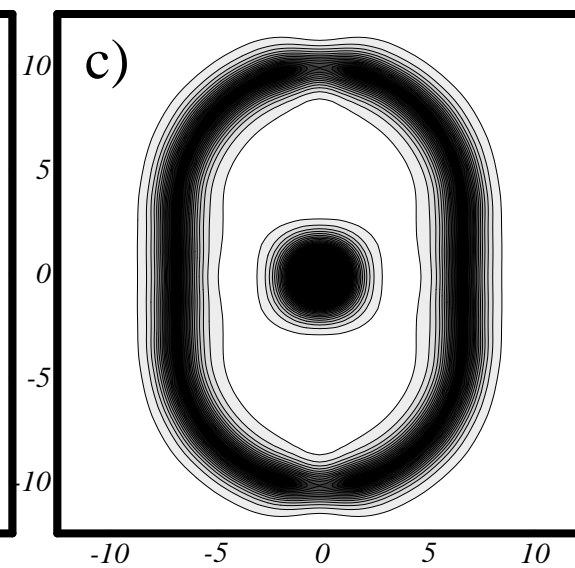
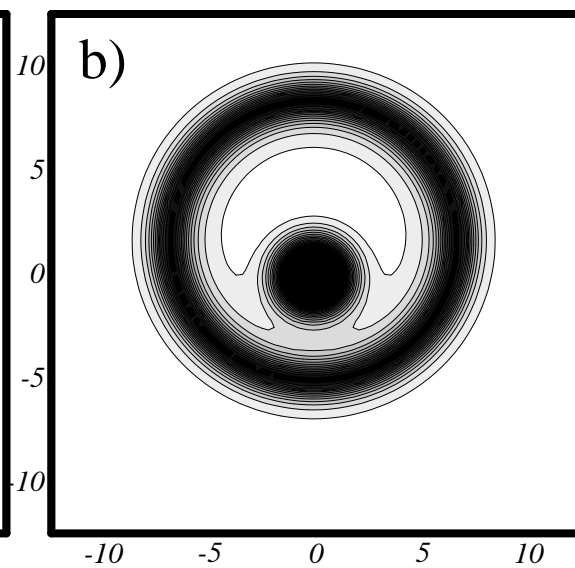
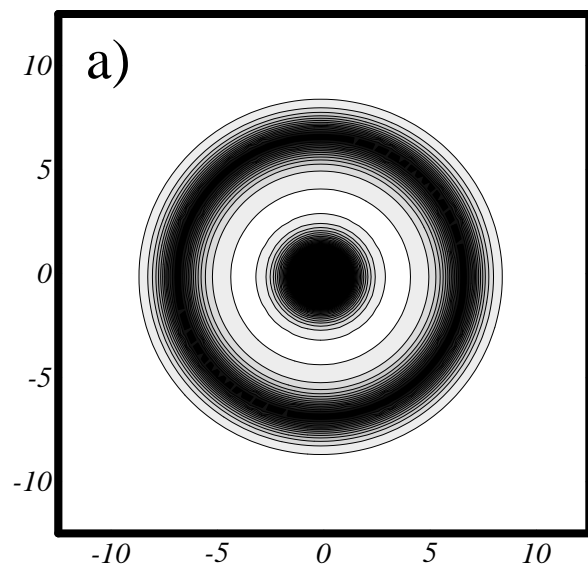
FIGURES

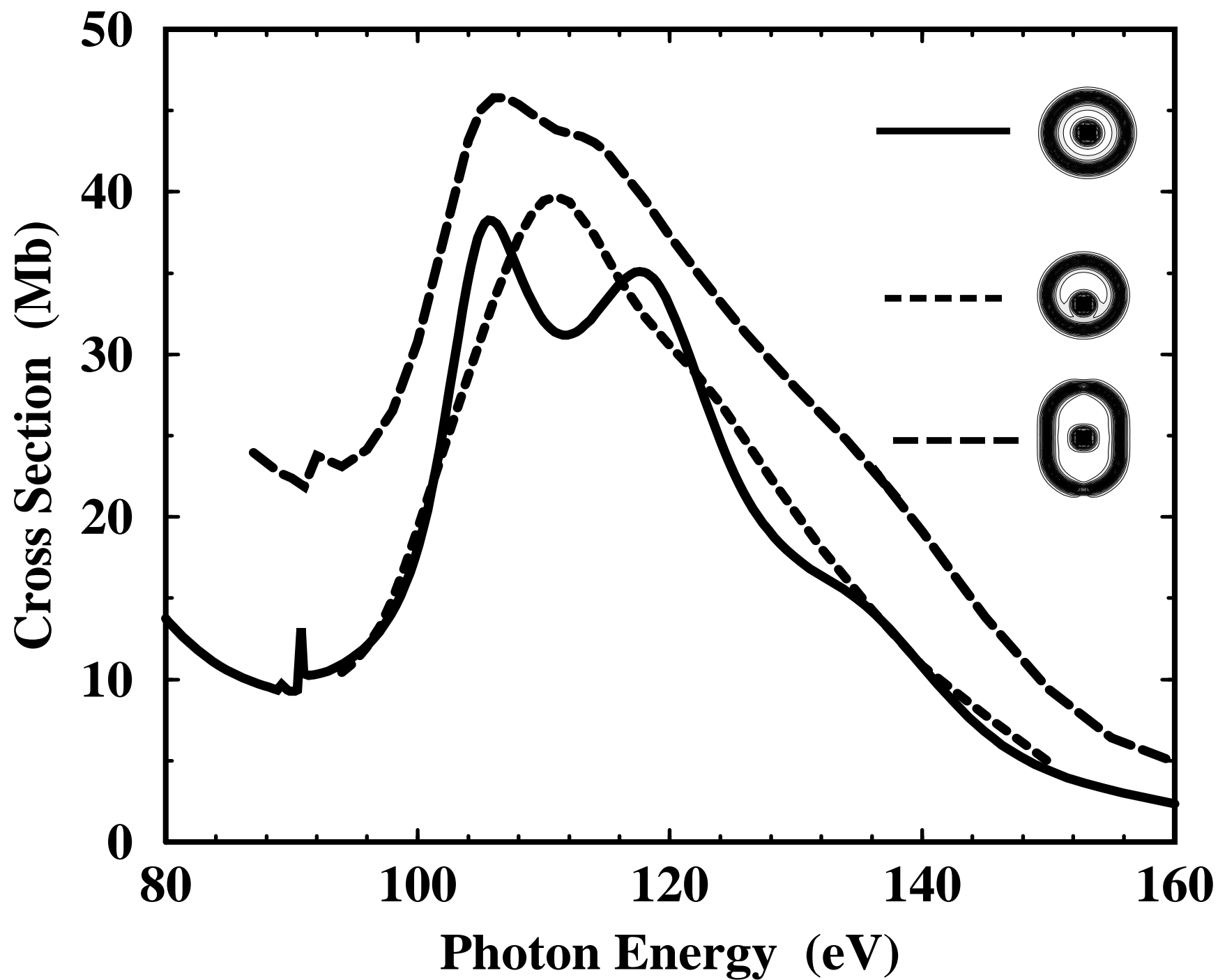
FIG. 1. Self-consistent charge density plots for $\text{Ba}@C_n$ metallofullerene model clusters (2D jellium model for the C_n nuclear charge; number of electrons chosen to give closed-shell electronic structure): (a) $\text{Ba}@C_{60}$: spherically symmetric C_{60} cage ($R=6.7$ a.u.; 56+230 electrons) with Ba at the center; (b) $\text{Ba}@C_{60}(C_{\infty v})$: spherically symmetric C_{60} cage ($R=6.7$ a.u.; 56+230 electrons) with Ba displaced 1.725 a.u. from the center; (c) $\text{Ba}@C_{90}(D_{\infty h})$: Ba at the inversion center of C_n cylinder with hemispherical C_{60} end caps ($R_{\text{cyl}} = 6.7$ a.u., total length=10.0 a.u.; 56+360 electrons).

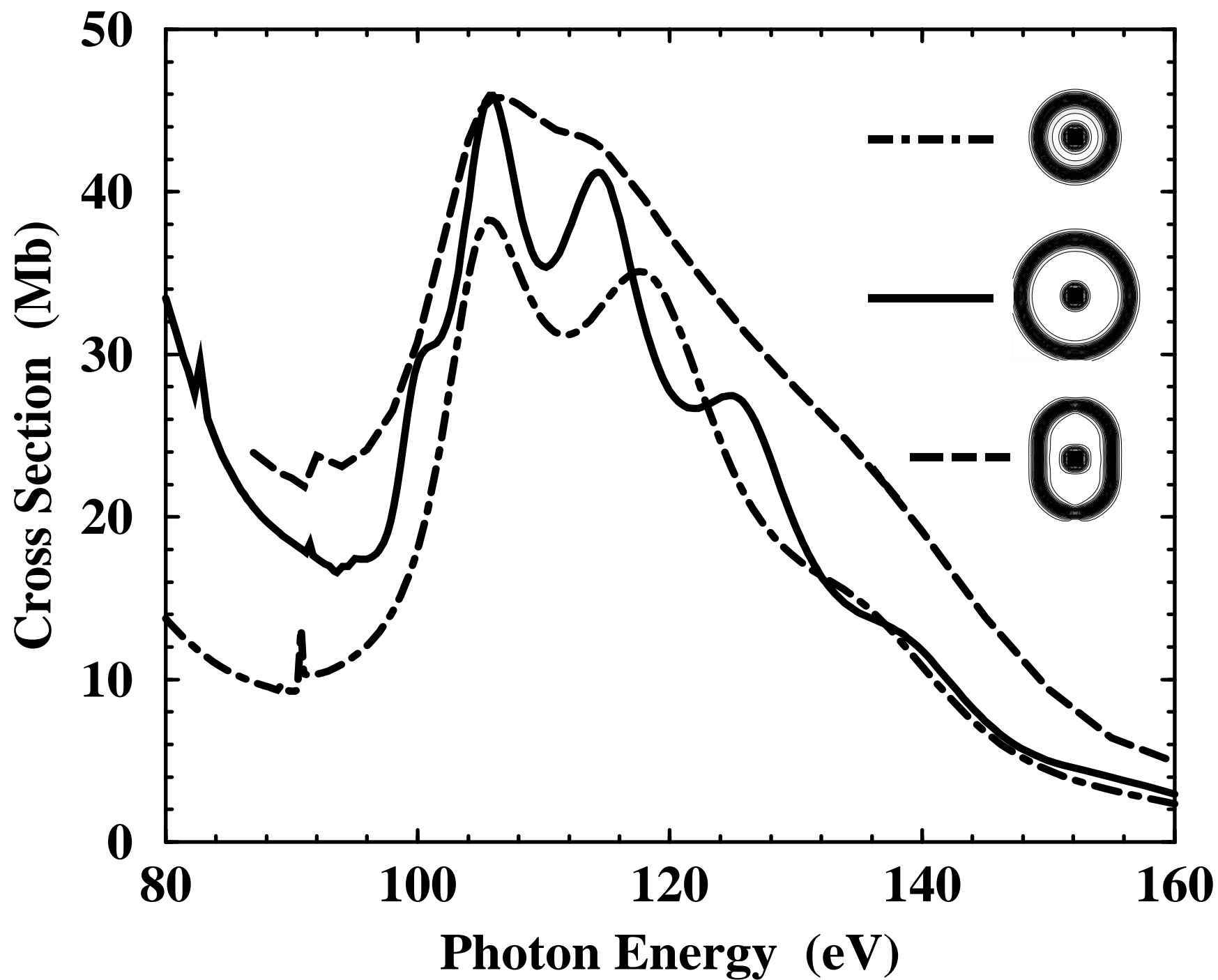
FIG. 2. Photoabsorption cross sections of the $\text{Ba}@C_n$ clusters defined in Fig. 1: Spherically symmetric $\text{Ba}@C_{60}$ ($E_{4d} = 90.4\text{eV}$); displaced Ba, $\text{Ba}@C_{60}(C_{\infty v})$ ($E_{4d} = 89.6\text{eV}$); elongated C_n , $\text{Ba}@C_{90}(D_{\infty h})$ ($E_{4d} = 91.6\text{eV}$). For comparison, $E_{4d} = 93.7\text{eV}$ in a free LDA Ba atom, and $E_{4d} = 93.3\text{eV}$ in selfconsistent (SCF) O-Ba-O (the result in Ref. [11] is not SCF). All calculated energies in this work are non-relativistic.

FIG. 3. Photoabsorption cross sections of $\text{Ba}@C_n$ clusters with an inversion center: Spherical $\text{Ba}@C_{60}$, non-spherical $\text{Ba}@C_{90}(D_{\infty h})$, and spherical $\text{Ba}@C_{130}$ ($E_{4d} = 94.3\text{eV}$).

FIG. 4. Partial photoionization cross sections of displaced $\text{Ba}@C_{60}(C_{\infty v})$ (see also Fig.1(b) and Fig.2). The 4d cross section is the sum of $4d\sigma$, $4d\pi$, and $4d\delta$ components with energy splitting ≈ 0.016 eV (≈ 0.055 eV in elongated $\text{Ba}@C_{90}$). The 5p cross section ($E_{5p} = 16.4\text{eV}$) is the sum of $5p\sigma$ and $5p\pi$ components with energy splitting ≈ 0.116 eV. The $5s\sigma$ level has binding energy $E_{5s} = 28.2\text{eV}$. The valence cross section represents the integrated emission from the occupied levels in the 3.14(HOMO)-8.60 eV range below the vacuum level.







Partial Cross Sections Ba@C₆₀

displaced 1.725 (a.u.)

